

## Vibrational and structural properties of tetramethyltin under pressure

Zhen-Xing Qin,<sup>1</sup> Xiao-Jia Chen,<sup>2,3</sup> Chao Zhang,<sup>4</sup> Ling-Yun Tang,<sup>1</sup> Guo-Hua Zhong,<sup>5</sup>  
Hai-Qing Lin,<sup>5,6</sup> Yue Meng,<sup>7</sup> and Ho-Kwang Mao<sup>2,3</sup>

<sup>1</sup>Department of Physics, South China University of Technology, Guangzhou 510640, China

<sup>2</sup>Geophysical Laboratory, Carnegie Institution of Washington, Washington, DC 20015, USA

<sup>3</sup>Center for High Pressure Science and Technology Advanced Research, Shanghai 201203, China

<sup>4</sup>Department of Physics, Yantai University, Yantai 264005, China

<sup>5</sup>Shenzhen Institutes of Advanced Technology, Chinese Academy of Sciences, Shenzhen 518055, China

<sup>6</sup>Beijing Computational Science Research Center, Beijing 100084, China

<sup>7</sup>HPCAT, Carnegie Institution of Washington, 9700 S. Cass Ave., Argonne, Illinois 60439, USA

(Received 25 September 2012; accepted 17 December 2012; published online 10 January 2013)

The vibrational and structural properties of a hydrogen-rich group IVa hydride,  $\text{Sn}(\text{CH}_3)_4$ , have been investigated by combining Raman spectroscopy and synchrotron x-ray diffraction measurements at room temperature and at pressures up to 49.9 GPa. Both techniques allow the obtaining of complementary information on the high-pressure behaviors and yield consistent phase transitions at 0.9 GPa for the liquid to solid and 2.8, 10.4, 20.4, and 32.6 GPa for the solid to solid. The foregoing solid phases are identified to have the orthorhombic, tetragonal, monoclinic crystal structures with space groups of  $Pmmm$  for phase I,  $P4/mmm$  for phase II,  $P2/m$  for phase III, respectively. The phases IV and V coexist with phase III, resulting in complex analysis on the possible structures. These transitions suggest the variation in the inter- and intra-molecular bonding of this compound.

© 2013 American Institute of Physics. [<http://dx.doi.org/10.1063/1.4774022>]

### I. INTRODUCTION

The tetra-alkyl compounds of group IVa elements have spurred a tremendous interest in the spectroscopy<sup>1–12</sup> due to their highly symmetrical characters. In the molecular structure of these compounds, the group IVa element is tetrahedrally coordinated by methyl groups ( $-\text{CH}_3$ ), making the molecule with the  $T_d$  symmetry.<sup>1,4</sup> Studies on the tetra-alkyl compounds of group IVa elements at low temperature conditions<sup>13–17</sup> suggested that the  $\text{CH}_3$  groups play a central role to understand the phase transitions and the  $\text{CH}_3$  groups become non-equivalent and exhibit intermolecular interactions.<sup>18,19</sup> Additionally, applying the pressure to the compounds, the  $\text{CH}_3$  group(s) show various behaviors. Under pressure, the rotational vibration of  $\text{CH}_3$  group(s) has been restricted in some  $\text{CH}_3$ -bearing compounds, such as  $\text{CH}_3\text{HgM}$  ( $\text{M}=\text{Cl}, \text{Br}, \text{I}$ )<sup>20</sup> and  $(\text{CH}_3)_2\text{XM}$  ( $\text{X}=\text{Sn}$  or  $\text{Tl}$ ).<sup>21,22</sup> The  $\text{CH}_3$  groups display different rotational angles in cubic  $\text{Si}(\text{CH}_3)_4$  at only 0.58 GPa.<sup>23</sup> Therefore, understanding the behavior of  $\text{CH}_3$  groups in the tetra-alkyl compounds of group IVa elements, especially the variance of  $\text{CH}_3$  groups under pressure, is important for condensed matter physics, materials science, and chemistry.

Group IVa hydrides also provide an alternative way to metallic hydrogen which was predicted to be a superconductor with high transition temperature in monatomic and molecular phases. In group IVa hydrides, the hydrogen atoms probably have undertaken chemical precompression by the group IVa atoms within the unit,<sup>24</sup> and thus the chemical pressure environments in these hydrides may greatly reduce the physical pressure necessary for metallic hydrogen. Many experimental and theoretical efforts are currently underway to investigate this prediction, such as  $\text{SiH}_4$ ,<sup>25–35</sup>  $\text{GeH}_4$ ,<sup>36–40</sup>

$\text{SnH}_4$ ,<sup>41–44</sup> and  $\text{PbH}_4$ .<sup>45</sup> However, very recently experiment shows the possible decomposition of  $\text{SiH}_4$  under irradiation from x-rays and lasers,<sup>46,47</sup> which makes the metallization of  $\text{SiH}_4$  extremely intangible and the stability of group IVa hydrides unprecedentedly important. Excitingly,  $\text{Si}(\text{CH}_3)_4$ , one of the tetra-alkyl hydrides of group IVa elements, was found no decomposition up to 142 GPa in our recent work,<sup>48</sup> although it remains unknown to metallize. Above 96 GPa, the sudden disappearing of original vibrational modes and appearing of the softening behavior from the new Raman modes makes the metallization of tetramethylsilane more complex. In addition, it is suggested that the homologous hydrides with heavier group IVa atoms would yield lower metallization pressure, due to the weaker chemical bonds which be dissociated under pressure.<sup>42</sup> Study on  $\text{Ge}(\text{CH}_3)_4$  by the Raman spectroscopy verified that high-pressure behaviors of  $\text{CH}_3$  groups do appear earlier with the compressed process despite uncertain to metallize.<sup>49</sup> Therefore, the investigation of heavier group IVa hydrides is in great demand.

In this paper we present the pressure-induced phase transitions of tetramethyltin (TMT),  $\text{Sn}(\text{CH}_3)_4$ , by Raman spectra and synchrotron powder x-ray diffraction. The fact that softening of the modes disappeared earlier besides of several possible phase transitions identified at 0.9, 2.8, 10.4, 20.4, and 32.6 GPa. Lattice vibrational modes in low frequency incidentally play a vital role to distinguish the phase transitions and corresponding reasonable phase structures also were determined by fitting the XRD patterns of TMT. Our findings have great implications for achieving metallization under high pressure based on hydrogen-rich compounds.

## II. EXPERIMENTAL DETAILS

TMT (*m.p.* 219 K, *b.p.* 347–348 K) as transparency liquid with 98% purity was purchased from Alfa-Aesar and used without further purification. The high-pressure experiments for TMT were carried out using DACs with beveled anvils and the culets of 200 micrometers. A hole of  $\sim 70$  micrometers in diameter drilled in a preindented tungsten gasket served as the sample chamber. To avoid volatilizing, the bottoms of the DACs were put into ice-water mixture half an hour before loading the sample. Liquid TMT was loaded into the chamber of the DACs with a syringe. Because of the liquid sample, no pressure medium was used and ruby grains had been placed previously for pressure calibration.

Raman spectra were obtained in a backscattering geometry with a spectrometer (with  $1800\text{ mm}^{-1}$  grating) equipped with a di-monochromator and a charge coupled device detector, giving a resolution of  $1\text{--}2\text{ cm}^{-1}$ . Radiation of  $532\text{ nm}$  from a solid-state laser ( $0.5\text{ W CW}$ ) was used for the excitation of the Raman spectra and all spectra were measured at ambient temperature. The scattering light was captured with a single exposure of the CCD with a spectral resolution of  $1\text{ cm}^{-1}$ .

The same DAC was employed for the high-pressure synchrotron XRD experiment. Considering the volatilizing of samples, pressure was increased to  $0.5\text{ GPa}$  after loading well the samples. Synchrotron radiation measurements with a wavelength of  $0.3986\text{ \AA}$  were performed at the 16-ID-B beamline of HPCAT, the Advanced Photon Source of the Argonne National Laboratory. The sample-to-detector distance and the image plate orientation angles were calibrated using  $\text{CeO}_2$  standard. The two-dimensional diffraction images were converted to  $2\theta$  versus intensity data plots using the FIT2D software.

## III. RESULTS AND ANALYSIS

### A. High-pressure Raman spectra of TMT

As shown in Fig. 1, in a single molecule of TMT, the tin atom is tetrahedrally bonded to four methyl groups. For ideally tetrahedral  $T_d$  ( $-43m$ ) molecular symmetry, one bond distance C–H, one Sn–C, and one Sn–C–H angle would describe fully the molecular geometry. The methyl groups can

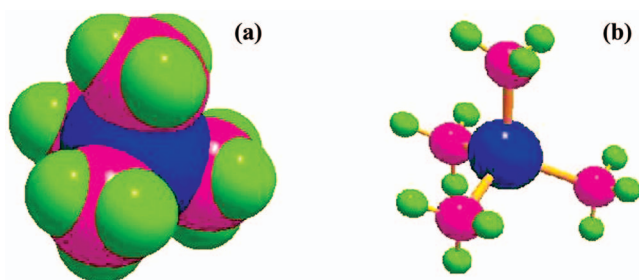


FIG. 1. The configurations of TMT with respect to ideally tetrahedral  $T_d$  ( $-43m$ ) symmetry. (a) Cup model of TMT shown to illustrate almost spherically shaped molecules in a close-packed stacking, and (b) ball-and-stick model of TMT manifested that one bond distance C–H, one Sn–C, one Sn–C–H/C–Sn–C angle could describe the molecular geometry.

be fully staggered with respect to the Sn–C bonds fully eclipsed or disordered (Fig. 1(b)). The irreducible representation (of all the normal vibrational modes) is  $\Gamma = 3A_1 + A_2 + 4E + 4F_1 + 7F_2$ . According to the selection rule, the  $A_1$ ,  $E$ , and  $F_2$  vibrations are Raman active. The type of vibrations was well assigned to each Raman signal of TMT at ambient conditions and is summarized in Table I. Our data at ambient pressure are in good agreement with the previous results.<sup>4,50</sup>

Figure 2 shows the selected Raman vibrational spectra of TMT as a function of pressure, which were collected from ambient pressure to  $49.9\text{ GPa}$ . Clearly, the Raman spectra could be divided into five regions based on the molecular nature of the complex: the C–Sn–C skeletal deformation region ( $100\text{--}500\text{ cm}^{-1}$ ), the C–Sn skeletal stretch region ( $500\text{--}650\text{ cm}^{-1}$ ), the  $\text{CH}_3$  rocking region ( $700\text{--}900\text{ cm}^{-1}$ ), the  $\text{CH}_3$  symmetrical deformation region ( $1100\text{--}1300\text{ cm}^{-1}$ ), and the  $\text{CH}_3$  symmetrical and nonsymmetrical stretch region ( $2900\text{--}3300\text{ cm}^{-1}$ ). With increasing pressure, all of the measured peaks shift to higher frequencies, and become weak at pressure up to  $49.9\text{ GPa}$ . Some of peaks nearly vanish except for the  $\nu_7 = 1410\text{ cm}^{-1}$  and  $\nu_8 = 1438\text{ cm}^{-1}$  (the  $\text{CH}_3$  nonsymmetrical deformation modes) which are influenced by the strong Raman signal of diamond at  $1332\text{ cm}^{-1}$ . This suggests that several pressure-induced phase transformations take place in TMT.

At ambient pressure, only one Raman signal appears in the C–Sn–C skeletal deformation region (Fig. 2), which is different from the low-Z compounds such as  $\text{Si}(\text{CH}_3)_4$  and  $\text{Ge}(\text{CH}_3)_4$ . The value of mode  $\nu_4$  is not precise enough in the  $\text{CH}_3$  rocking region due to the weak and broad inherent Raman signal, whereas it is very hard to be observed in foregoing experiment on  $\text{Ge}(\text{CH}_3)_4$ ,<sup>49</sup> compared to the work on  $\text{Si}(\text{CH}_3)_4$  which is clear to achieve the value of the mode  $\nu_5$ .<sup>48</sup> At the onset of compression, the intensities of the  $\nu_5$  and  $\nu_6$  modes exhibit a reversal change, which is an evidence for  $\nu_5$  and  $\nu_6$  modes to exchange of the symmetry assignment of these two modes as a result of Fermi resonance,<sup>51</sup> and a new mode is extruded in the middle of the  $\nu_5$  and  $\nu_6$  modes, which is labeled as mode  $\nu_6'$ . Compressed to  $0.9\text{ GPa}$ , a lattice vibrational mode (lattice mode 1) emerges at the low-frequency region of  $\sim 110\text{ cm}^{-1}$ . The emergence of new vibrational modes, especially the lattice mode, can be identified to the liquid-solid state transition upon application of the external pressure. With further compression, the mode  $\nu_2$  and  $\nu_3$  also perform the reversal change in intensity and a weak mode ( $\nu_5'$ ) appears at the low frequency of the mode  $\nu_5$ . Application pressure to  $2.8\text{ GPa}$ , the mode extruded in the middle of the  $\nu_5$  and  $\nu_6$  modes suddenly disappears besides of the further increasing relative intensity of mode  $\nu_2$  and  $\nu_3$ . This suggests that TMT undergoes a possible pressure-induced phase transition. Upon further compression up to  $10.4\text{ GPa}$ , three other modes emerge, a new mode ( $\nu_4'$ ) in the region of the  $\text{CH}_3$  rocking and two new modes in the  $\text{CH}_3$  symmetrical and nonsymmetrical stretch region. The mode slightly located on the shoulder of the mode  $\nu_9$  is labeled as mode  $\nu_9'$ . In addition, the relative intensity of the mode  $\nu_2$  and  $\nu_3$  yet recovers to the case of ambient conditions and the mode  $\nu_5'$  disappears soon. Such rich Raman features suggest the existence of another new phase. With increasing pressure to  $19.3\text{--}20.4\text{ GPa}$ ,



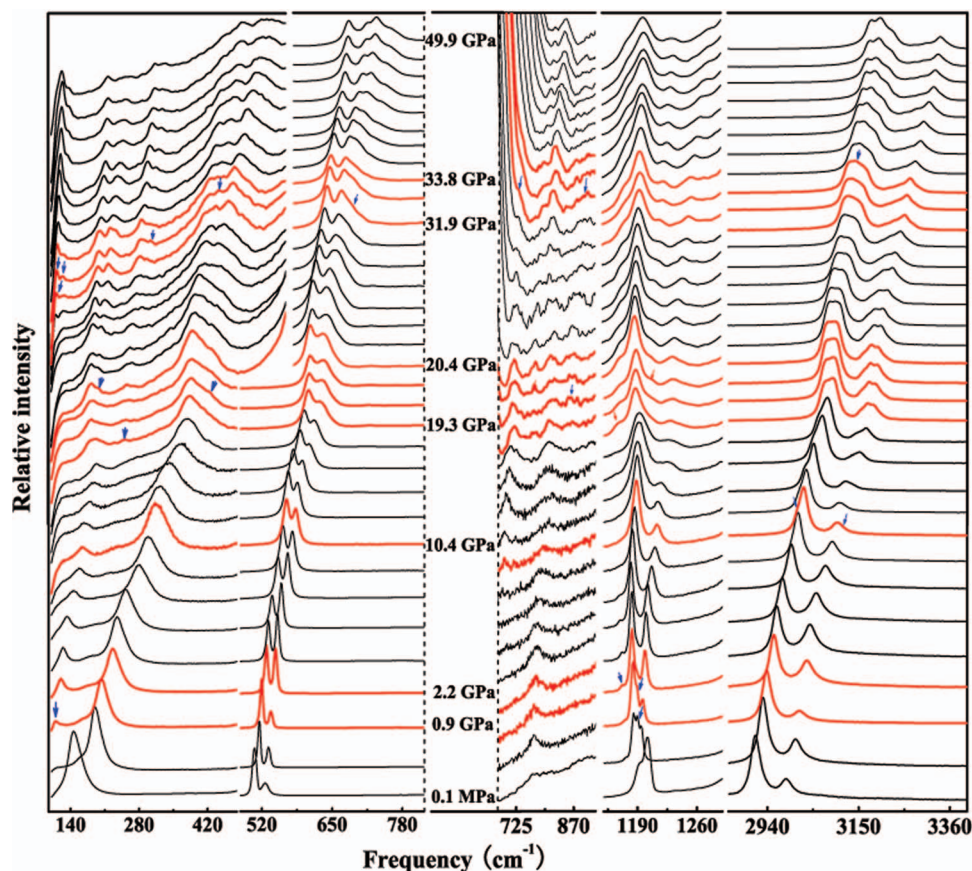


FIG. 2. Representative Raman spectra of TMT in the full spectral regions at ambient conditions upon compression to 49.9 GPa. The blue arrows labeled are to make the change of part Raman modes clear to observe. The value of pressure is labeled only on red spectra to exhibit clearly the possible phase transitions.

adjacent mode of mode  $\nu_9'$ . Proceeding with compression to 49.9 GPa, no change has been observed from all the modes, only accompanied by weakening and broadening of modes.

Vibrational frequencies provide information of the high-pressure behavior of TMT. To show the possible phase transitions on compression, the pressure dependences of Raman modes are depicted in Fig. 3. Reasonably, there are several distinct pressure regions in Fig. 3, which are labeled as liquid phase (below 0.9 GPa), phase I (0.9–2.8 GPa), phase II (2.8–10.4 GPa), phase III (10.4–19.3 GPa), phase IV (20.4–31.9 GPa), and phase V (above 32.6 GPa). For the liquid phase of TMT, nearly all the modes exhibit the blue-shift with increasing pressure, whereas the  $\nu_5$  and  $\nu_6$  modes show a softening behavior, which is a typical character of rotational mode of the  $\text{CH}_3$  group.<sup>20–22</sup> Due to pressure-induced increase of intra- and inter-molecular interaction, equivalent  $\text{CH}_3$  groups would not remain stable and rotate by certain angles, which is inevitable to lead to changes of crystal structure.<sup>23</sup> In the phase I, partial modes in the  $\text{CH}_3$  symmetrical deformation region are still softening with increasing pressure, which could be observed in Fig. 3 until the phase II. This phenomenon, especially transient phase I, implies the sensitive pressure effect of  $\text{CH}_3$  groups. With further increasing pressure, twisted structure of TMT molecule again is stretched by external pressure, which has resulted in the changes of the stretch modes of TMT in phase III. At compression up to 20.4 GPa, the number of the Raman modes increases greatly in the high-

pressure phases IV, which indicates the new phase with lower symmetry. Furthermore, new modes emerge in the C–Sn–C skeletal deformation and C–Sn skeletal stretch region suggests further compression has already taken effect inside the molecule. For the phase V, although compression still leads other new modes to appear, the vanishing of modes implies related atoms are governed partly and it would be possible to conform the closer-packing atomic layer(s).

Phase transformations are further identified by the changes of pressure coefficients. The fitted pressure coefficients ( $d\nu/dP$  ( $\text{cm}^{-1}/\text{GPa}$ )) of the monitored peaks obtained by linear regression are listed in Table I. In general, most of the pressure coefficients of the vibrational modes decrease noticeably with increasing pressure, and negative pressure-coefficients of the modes in the  $\text{CH}_3$  symmetrical deformation region again show the softening behavior of TMT at the pressure. From the liquid phase to phase I, the value of  $d\nu/dP$  of the modes  $\nu_5$  and  $\nu_6$  changes from negative to positive, indicating the rotational motion of the  $\text{CH}_3$  groups is compelled to be frozen in positions.<sup>51</sup> The case has also happened in the high-pressure experiments of the homomolecular compounds,  $\text{Si}(\text{CH}_3)_4$ <sup>48</sup> and  $\text{Ge}(\text{CH}_3)_4$ .<sup>49</sup> However, for the  $\text{Si}(\text{CH}_3)_4$ , this softening behavior exists with the pressure up to 9.0 GPa and the related modes still exist in the whole pressure region of 30 GPa. Recent work on  $\text{Ge}(\text{CH}_3)_4$  showed softening behavior could be kept to 1.4 GPa and the related modes disappeared at around 5 GPa. Here, it is only at 0.9 GPa that soft-

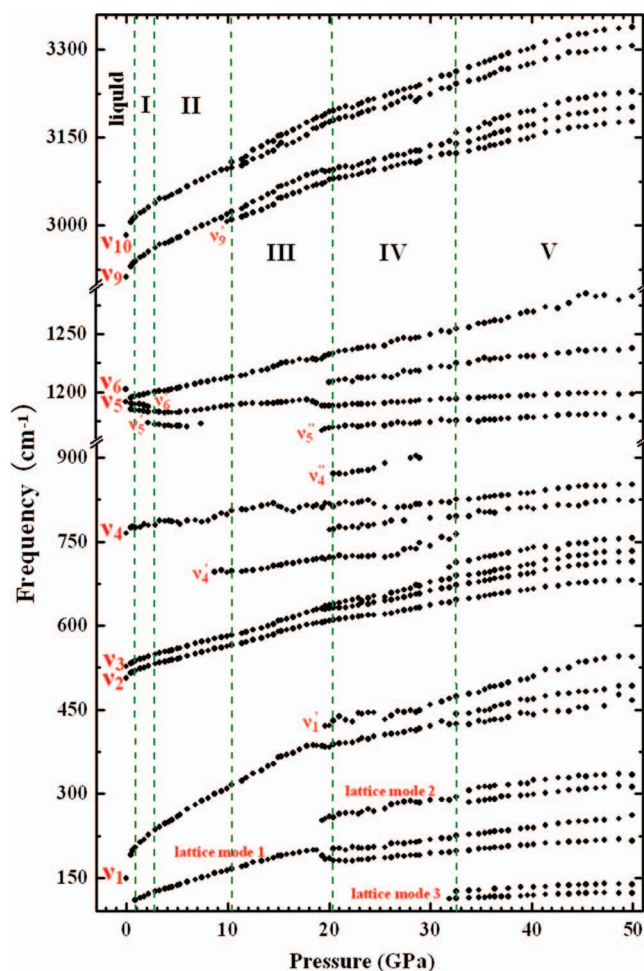


FIG. 3. Pressure dependence of the frequencies of TMT for the observed modes in all regions at room temperature. The vertical dashed lines at near 0.9, 2.8, 10.4, 20.4, and 32.6 GPa indicate the proposed phase boundaries.

ening behavior exists, whereas the related modes are also kept in the whole pressure region of 49.9 GPa. In phase I and II, the modes  $\nu_5'$  and  $\nu_6'$  of TMT also undergo softening, but their  $d\nu/dP$ s are larger than those of the  $\nu_5$  and  $\nu_6$  modes, manifesting that new high-pressure structures are prone to be compressed. Interestingly, there is an unusual case that high-pressure phase III possesses unexpected higher compressibility for most of the modes than that of phase II, which is also observed in the phase V that several modes exhibit higher compressibility. This provides powerful evidence of phase transition.

## B. Structural transformation of TMT under pressure

Synchrotron powder x-ray diffraction measurements on TMT were performed to determine detailed structural information for the possible phases at high pressures. Figure 4 shows the x-ray diffraction patterns of TMT at pressures up to 38.2 GPa. All the Bragg peaks shift to larger angles, showing the shrinkage of TMT lattice. From 1.8 to 3.2 GPa, the relative intensities of several peaks change and new peaks grow. There are some disappeared peaks around  $10^\circ$  besides of the change in the relative intensities. The appearance of the new signals from the new phase can be observed around  $11.5^\circ$ . This indicates a phase transition, which coincides with the

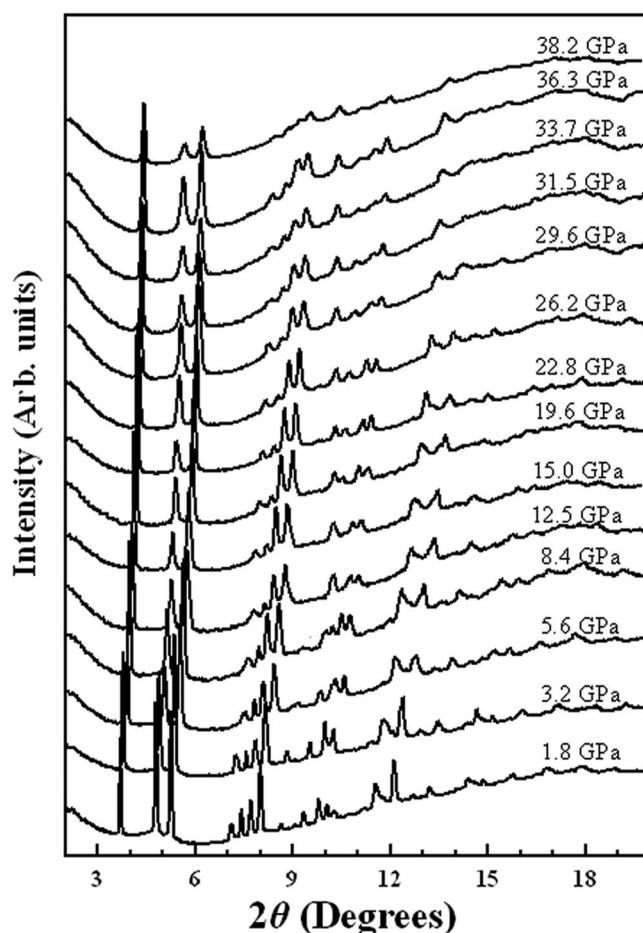


FIG. 4. Synchrotron radiation x-ray ( $\lambda = 0.3986 \text{ \AA}$ ) diffraction patterns of TMT during the pressurization from ambient conditions to 38.2 GPa.

Raman result of the phase transition at 2.8 GPa. With continuous compression to 12.5 GPa, a weak peak appears around  $13.5^\circ$  and some signals happen to vanish, implying that TMT undergoes a phase transition. This phase corresponds to the phase III observed in Raman spectroscopy above 10.4 GPa. Further compression to 38.2 GPa, the diffraction patterns become significantly broader, and additional weak peaks appear at 19.6 GPa, signaling a phase transition consisting with the Raman results of a phase transition at 20.4 GPa. However, all peaks still remain their original forms with increasing pressures. It is therefore difficult to determine the phase transition of the phase V.

To investigate the crystal structure of each phase, the diffraction patterns obtained at selected pressures were indexed using DICVOL04 and refined using the Le Bail method with GSAS software.<sup>52</sup> For phase I, indexing yields a unique solution, which leads to an orthorhombic cell (space group  $Pmmm$ ) with lattice parameters  $a = 10.5290(8) \text{ \AA}$ ,  $b = 7.5529(6) \text{ \AA}$ , and  $c = 4.7720(4) \text{ \AA}$  at 1.8 GPa. The phase I was fitted with the space group of  $Pmmm$ , and the measured and fitted data are shown in Fig. 5(a). As seen in Fig. 5(a), the positions and intensities of the diffraction peaks of TMT at 1.8 GPa are fitted well within the indexed structures. Phase II of TMT is indexed with a tetragonal cell (space group  $P4/mmm$ ) with lattice parameters  $a = 10.4423(8) \text{ \AA}$ ,

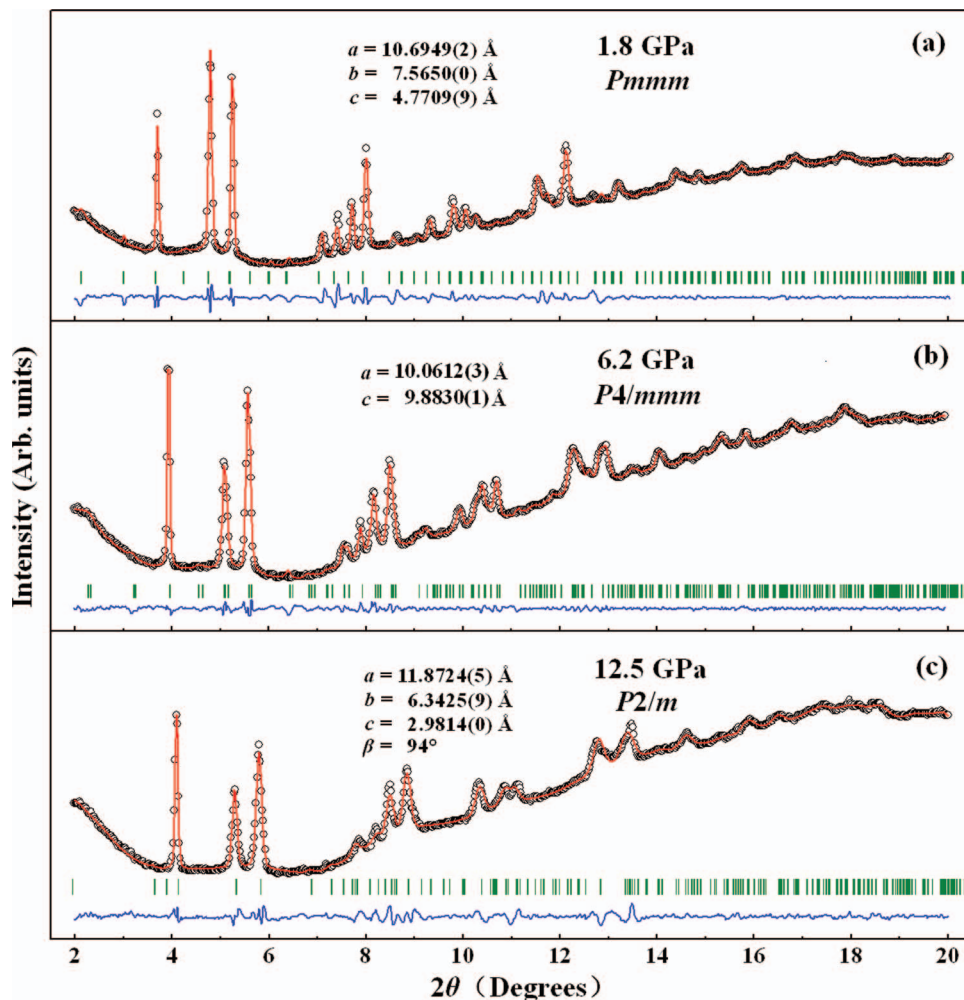


FIG. 5. X-ray powder diffraction patterns of liquid TMT at pressures of (a) 1.8, (b) 6.2, and (c) 12.5 GPa, respectively. The refined lattice parameters for the corresponding space groups are given, respectively. The open circles represent the measured intensities and the red lines the results of profile refinements by the best LeBail-fit with each space group. The positions of the Bragg reflections are marked by vertical lines and the difference profiles are shown at the bottoms (blue lines). The  $R$  values are  $R_p = 0.4\%$ ,  $R_{wp} = 0.7\%$  for the fitting at 1.8 GPa,  $R_p = 0.2\%$ ,  $R_{wp} = 0.3\%$  at 6.2 GPa, and  $R_p = 0.3\%$ ,  $R_{wp} = 0.4\%$  at 12.5 GPa.

$c = 10.3013(2)$ , and  $V = 1123.29 \text{ \AA}^3$  at 3.2 GPa. Other possible symmetries such as orthorhombic and monoclinic cells are also gotten simultaneously and an orthorhombic cell even has a more reasonable *figure of merit* ( $M$ ,  $F$ ); however, the results by fitting the patterns in phase II with space group  $P4/mmm$  achieve the best anastomotic effect. Figure 5(b) shows the result of fitting the patterns at 6.2 GPa. The space groups of phase I and II are very rare compared to the structures of  $\text{Si}(\text{CH}_3)_4$  and  $\text{Ge}(\text{CH}_3)_4$  under pressure.<sup>23,49</sup> Although phase III of TMT is indexed with an orthorhombic cell and all kinds of the monoclinic cell at 12.5 GPa, the monoclinic symmetry would be unique for phase III due to the unsuitable volume of the orthorhombic cell. Furthermore, it is quite interesting to notice that all the monoclinic cells are characterized by different lattice parameters and the same space group  $P2/m$  at this pressure. It might be reasonable to take the lattice parameters  $a = 11.8438(2) \text{ \AA}$ ,  $b = 6.3170(8) \text{ \AA}$ ,  $c = 2.9825(7) \text{ \AA}$ , and  $\beta = 94.101(8)^\circ$  with the volume of  $222.57 \text{ \AA}^3$  because of a remarkably good value of the *figure of merit* ( $M$ ,  $F$ ) at this pressure. Figure 5(c) shows the measured and fitted patterns of TMT at 12.5 GPa. All diffraction patterns up to 19.6 GPa could be indexed with this cell. Above this pressure, all the

diffraction peaks, except for the additional peaks, could still be fitted with the monoclinic cell. This suggests that above 19.6 GPa, the structure of phase III either becomes more complex or coexists with an appearing new high-pressure phase. Drastic Raman spectra change coincidentally in the pressure region of 19.3–20.4 GPa, especially the observation of abundant new internal modes. This strongly suggests that an enhanced intermolecular interaction with covalent nature results in the complex crystal structures.

Although the usage of the Le Bail method can give reasonable spaces groups and yields accurate lattice parameters of the structures, this method has not provided any information about the internal coordinates. Since the obtained data are not sufficiently detailed for a Rietveld fit, we now perform theoretical calculations to provide the detailed information.

Table II summarizes the calculated lattice parameters and atomic coordinates of the experimentally obtained phases with the space groups of  $Pmmm$ ,  $P4/mmm$ , and  $P2/m$  at pressures of 1.8, 3.3, and 12.5 GPa, respectively. Comparing with the corresponding phases with experimental data, the crystal lattice parameters are well consistent. There has been no

TABLE II. Calculated lattice parameters and atomic coordinates of the experimentally obtained phases with the space groups of  $Pm\bar{m}m$ ,  $P4/m\bar{m}m$ , and  $P2/m$  at pressures of 1.8, 3.2, and 12.5 GPa, respectively.

Lattice parameters	Atomic coordinates (fractional)
<b><math>Pm\bar{m}m</math> (<math>Z = 2</math>)</b>	
$a = 10.6949 \text{ \AA}$	Sn 2l (0.3862, 0.5000, 0.5000)
$b = 7.5650 \text{ \AA}$	C 4z (0.6820, 0.2308, 0.5000)
$c = 4.7709 \text{ \AA}$	C 4x (0.8710, 0.5000, 0.6594)
$\alpha = 90^\circ$	H 8A (0.7371, 0.2015, 0.3110)
$\beta = 90^\circ$	H 8A (0.9167, 0.3823, 0.7456)
$\gamma = 90^\circ$	H 4z (0.5977, 0.1477, 0.5000)
	H 4x (0.7789, 0.5000, 0.7640)
	Sn 8r (0.2366, 0.2366, 0.2516)
	C 16u (0.3631, 0.1370, 0.6393)
	C 8r (0.3588, 0.3588, 0.8357)
	C 8r (0.1314, 0.1314, 0.8670)
	H 16u (0.3152, 0.0733, 0.5732)
	H 16u (0.4228, 0.0826, 0.7057)
	H 16u (0.4198, 0.2063, 0.5853)
	H 16u (0.3280, 0.5586, 0.7819)
	H 16u (0.1977, 0.9233, 0.9247)
	H 8r (0.3842, 0.6158, 0.9339)
	H 8r (0.0711, 0.9289, 0.8098)
	Sn 2n (0.2480, 0.5000, 0.5096)
	C 4o (0.3765, 0.7484, 0.6398)
	C 4o (0.1235, 0.7494, 0.6465)
	H 4o (0.4092, 0.8275, 0.3565)
	H 4o (0.4437, 0.6661, 0.8366)
	H 4o (0.3306, 0.8575, 0.8397)
	H 4o (0.0578, 0.6663, 0.8143)
	H 4o (0.0886, 0.8378, 0.3591)
	H 4o (0.1745, 0.8503, 0.8749)
<b><math>P4/m\bar{m}m</math> (<math>Z = 8</math>)</b>	
$a = b = 10.4063 \text{ \AA}$	
$c = 10.2438 \text{ \AA}$	
$\alpha = 90^\circ$	
$\beta = 90^\circ$	
$\gamma = 90^\circ$	
<b><math>P2/m</math> (<math>Z = 2</math>)</b>	
$a = 11.8438 \text{ \AA}$	
$b = 6.3417 \text{ \AA}$	
$c = 2.9825 \text{ \AA}$	
$\alpha = 90^\circ$	
$\beta = 94^\circ$	
$\gamma = 90^\circ$	

much effort in searching for more stable structures from the theoretical aspect. Our calculations indeed reveal that the experimentally determined structures are the competitive phases having the low enthalpies at zero temperature. Here the first-principles calculations were used to obtain the structural information within the framework of density-functional theory. The underlying structural relaxation has been performed with the VASP code<sup>53</sup> employing the projector augmented-wave pseudopotential<sup>54</sup> and the exchange correlation functional with the local density approximation.<sup>55</sup> The energy cutoff used in our calculations for the plane-wave basis set is 600 eV. In optimization calculation, a  $3 \times 3 \times 3$  k-mesh was used for the sampling of the Brillouin zone. We optimized the atomic positions until the forces acting on the atoms are smaller than 0.02 eV/Å. And the convergence tolerance of the total energy is  $10^{-5}$  eV/unit cell.

The band structure calculations reveal the insulating feature of the two low-pressure structures at 1.8 and 3.2 GPa. The electronic band structure of the  $P2/m$  phase at 12.5 GPa is shown in Fig. 6(a). The calculations yield the metallic character with large dispersion bands crossing the Fermi level. Three bands were found to contribute the metallic behavior through the cross of the Fermi level around F and Q points and two different parallel bands along the  $Q \rightarrow Z$  and  $Z \rightarrow \Gamma$  directions. The occurrence of parallel bands in the electronic band structure is a sign of possible nesting of two Fermi surfaces.

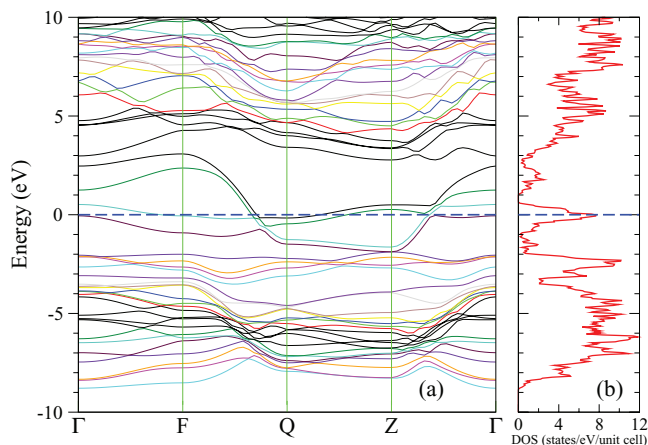


FIG. 6. Electronic band structure (a) and projected density of states (b) of the  $P2/m$  TMT at 12.5 GPa. The dashed lines represent the Fermi levels.

The projected density of states (DOS) shown in Fig. 6(b) further reveals the metallic properties of the  $P2/m$  phase at 12.5 GPa. At this pressure, the DOS is about 7.0 states/eV/unit cell at the Fermi level. Interestingly, the electrons dominate the energy range from  $-2$  to  $-11$  eV. The DOS increases gradually from 3 eV on above the Fermi level. These theoretical results are encouraging for the experimental detection of the metallization in such materials. Although our optical observations seemingly do not support the metallization in TMT, the resistance measurements on a similar aromatic hydrocarbon indeed revealed the metallic state at much low pressure of 40 GPa than that people generally thought.<sup>56</sup> Further resistance measurements are expected on this studied material.

#### IV. DISCUSSION

Lattice modes of TMT under pressure play an important role in analyzing the phase transitions. As seen in Fig. 2, the most prominent peaks in the whole region of pressure are lattice modes, which did not appear in high-pressure Raman spectra of  $\text{Si}(\text{CH}_3)_4$ .<sup>48</sup> The similar lattice modes were observed in Raman spectra of  $\text{Ge}(\text{CH}_3)_4$ .<sup>49</sup> However, these modes disappeared in phase IV even though only one appeared in the whole pressure region. More lattices vibrational modes of TMT under pressure appearing with compression suggests different course of the phase transitions. This provides the support for understanding the structures by fitting the XRD patterns of TMT under pressures. It has been reported that  $\text{Si}(\text{CH}_3)_4$  and  $\text{Ge}(\text{CH}_3)_4$  possibly underwent similar structure transformations<sup>14</sup> and these structures have also been proved reasonable.<sup>49</sup> The different new structures (i.e.,  $Pm\bar{m}m$  and  $P4/m\bar{m}m$ ) of TMT are observed at pressures. Theoretical efforts on group-14 hydrides ( $\text{XH}_4$ , X=C, Si, Ge, Sn, Pb) showed that  $\text{SnH}_4$  underwent metallic state with different structures ( $P6/m\bar{m}m$ ,<sup>42</sup>  $\text{Ama}2$ , and  $P6_3/m\bar{m}c$ .<sup>43,44</sup>).  $\text{SnH}_4$  has been predicted to achieve higher superconducting critical temperature<sup>42,44</sup> despite the occurring decomposition at low pressure. The decomposition has also been observed in group-14 hydrides such as  $\text{SiH}_4$ <sup>46,47</sup> and  $\text{GeH}_4$ .<sup>57</sup> Fortunately, we observe that most Raman modes of TMT keep blue shift until 49.9 GPa. This indicates that TMT would still be in per-

fect crystal states after undergoing some high-pressure phase transitions.

Structural transformation at different temperatures and pressures has been a critical issue to explore the feasibility of metallic hydrides. Compared to  $\text{Si}(\text{CH}_3)_4$  and  $\text{Ge}(\text{CH}_3)_4$  under pressure, TMT exhibits richer phase transitions at low pressures. This feature suggests that TMT may be easy to be compressed. Especially for the  $\text{CH}_3$  groups, no rotational mode in intrinsic spherically shaped molecules of TMT at ambient conditions is assigned, yet it exhibits softening related to the rotation of the  $\text{CH}_3$  group(s),<sup>20–22</sup> which is resulted possibly from the increasing intermolecular interaction of TMT, for example, Van der Waals.<sup>58</sup> Due to the shifting to blue-shift for softening modes, the external pressure undoubtedly makes the  $\text{CH}_3$  groups of TMT locked in the positions and restricts the rotation of the  $\text{CH}_3$  groups. Considering further phase transitions, it is uncertain whether all hydrogen atoms are built up in a network structure by means of the closest packing,<sup>24,29,33</sup> which has significant implications for metallic hydrogen under high pressure. The high-pressure behaviors of TMT, especially its stability and rich phases, manifest themselves as a candidate of hydrogen-rich material for achieving metallization at high pressure.

To reveal the compressibility of each phase, the lattice parameters and volume per formula unit were computed by fitting the patterns at selected pressures from the GSAS software.<sup>52</sup> Figure 7 plots the pressure dependence of the volume per formula unit as a function of pressure for each phase. For phase IV and V, we select the  $P2/m$  space group as possible crystal structure which is more reasonable under pressure. The volume/pressure relationship represents the equation of state (EoS), which can be described analytically by series expansions of Eulerian finite strain such as the Birch-Murnaghan equation of state (BM3 EoS)<sup>59</sup> defined as

$$P = 3K_0 f_E (1 + 2f_E)^{5/2} \left[ 1 + \frac{3}{2}(K'_0 - 4)f_E \right],$$

where  $f_E = [(V_0/V)^{2/3} - 1]/2$ ,  $V_0$  is the volume at ambient pressure,  $V$  is the volume at pressure  $P$  given in GPa,  $K_0$  is the bulk modulus, and  $K'_0$  is the first pressure derivative of  $K_0$ . The solid line in Fig. 7 represents the fitted results. The bulk modulus of the high-pressure phases (phase II–V) is  $11.18 \pm 4.02$  GPa with  $K'_0 = 5.40 \pm 0.91$ ,  $V_0 = 165.60 \pm 5.68 \text{ \AA}^3$ . The value of  $K_0$  suggests that high-pressure crystallized TMT is still soft, which enables the exploring of metallized TMT by the further compression. Compared to  $\text{Ge}(\text{CH}_3)_4$ ,<sup>49</sup> the increased bulk modulus of TMT infers an enhancement of bond strength during phase transitions, indicating the intrinsic high compressibility. These results suggest that the crystal structure has been entirely transformed with close-packing hydrogen and layered network would be possible.<sup>14</sup> The layered crystal structure for hydrogen atoms has been suggested to be essential metallic state in hydrogen-rich compounds.<sup>25,29,38,42,60</sup> Furthermore, the bulk modulus of TMT under pressure is remarkable strength because silane ( $\text{SiH}_4$ ) has gotten the bulk modulus of 7.89 GPa upon compression up to 39 GPa<sup>28</sup> and  $\text{SiH}_4\text{-H}_2$  complex has also achieved the value of 6.87 GPa with pressure up to 35 GPa,<sup>61</sup> whereas molecular hydrogen ( $\text{H}_2$ ) gets the value of

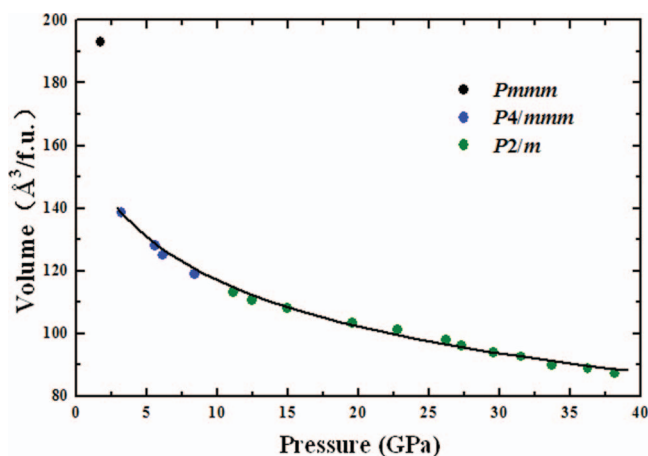


FIG. 7. Volume per formula unit change of TMT with pressure. The solid lines demonstrate the fitting data of phase to the Birch-Murnaghan equation of state.

only 0.16–0.36 GPa when being compressed to 23 GPa.<sup>62–65</sup> So far, there is little information on such a magnitude of hydrogen-bearing compound TMT. Measurements of electronic transport properties are expected to examine whether TMT would undergo the metallization and eventually become a superconductor at high pressures. It should be noticed that a recent electronic transport study on molecular hydrogen has reported a significant resistance drop at 260–270 GPa.<sup>66</sup> However, two independent measurements<sup>67,68</sup> indicate that metallic hydrogen has not been reached yet even at 360 GPa. The softening of some Raman modes on  $\text{CH}_3$  groups and their sudden disappearance in TMT indicate that this compound might be ideal for metallization and even high-temperature superconductivity at static pressure for laboratory capability.

## V. CONCLUSIONS

In conclusion, high-pressure spectroscopy has been used to characterize the high-pressure behavior of TMT. Our results revealed the phase transitions at 0.9, 2.8, 10.4, 20.4, and 32.6 GPa from the mode frequency shifts with pressure. We found that phase transitions of TMT are more sensitive to pressure than those of  $\text{Si}(\text{CH}_3)_4$  and  $\text{Ge}(\text{CH}_3)_4$ . These transitions were suggested to result from the changes in the inter- and intra-molecular bonding of this material. Further work using synchrotron X-ray radiation revealed similar results of phase transitions from Raman measurements and higher-pressure phases IV and V, however, possibly coexist with phase III. The space groups for the high-pressure phases were determined as following:  $Pmmm$  for phase I,  $P4/mmm$  for phase II, and  $P2/m$  for phase III. The equations of state were obtained up to 38.2 GPa. Such structural information may be helpful in exploring possible superconductivity in hydrogen-bearing compounds at high pressures.

## ACKNOWLEDGMENTS

X.J.C. and H.K.M. acknowledge eFree, an Energy Frontier Research Center funded by DOE-BES under Grant No. DE-SC0001057 for the structure measurements. The Raman

measurements and theoretical calculations in China were supported by the Cultivation Fund of the Key Scientific and Technical Innovation Project Ministry of Education of China (No. 708070), the Shenzhen Basic Research Grant (No. JC201105190880A), the National Natural Science Foundation of China (No. 11274335), Guangdong Natural Science Foundation (No. S2012040007929), and the Fundamental Research Funds for the Central Universities SCUT (No. 2012zz0078). The use of HPCAT, APS is supported by Carnegie Institution of Washington, Carnegie DOE Alliance Center, University of Nevada at Las Vegas, and Lawrence Livermore National Laboratory through funding from DOE–National Nuclear Security Administration, DOE–Basic Energy Sciences, and NSF. APS is supported by DOE–BES, under Contract No. DE-AC02-06CH11357.

- <sup>1</sup>C. W. Young, J. S. Koehler, and D. S. McKinney, *J. Am. Chem. Soc.* **69**, 1410 (1947).
- <sup>2</sup>K. Shimizu and H. Murata, *J. Mol. Spectrosc.* **5**, 44 (1961).
- <sup>3</sup>J. Overend and J. R. Scherer, *J. Opt. Soc. Am.* **50**, 1203 (1960).
- <sup>4</sup>F. Watari, *Spectrochim. Acta. A* **34**, 1239 (1978).
- <sup>5</sup>K. W. F. Kohlrausch and D. Barnes, *An. R. Soc. Esp. Fis. Quim.* **30**, 733 (1932).
- <sup>6</sup>D. H. Rank, *J. Chem. Phys.* **1**, 572 (1933).
- <sup>7</sup>D. H. Rank and E. R. Bordner, *J. Chem. Phys.* **3**, 248 (1935).
- <sup>8</sup>T. F. Anderson, *J. Chem. Phys.* **4**, 161 (1936).
- <sup>9</sup>J. T. Edsall, *J. Chem. Phys.* **5**, 225 (1937).
- <sup>10</sup>R. K. Sheline and K. S. Pitzer, *J. Chem. Phys.* **18**, 595 (1950).
- <sup>11</sup>S. Silver, *J. Chem. Phys.* **8**, 919 (1940).
- <sup>12</sup>S. Perry and J. Jonas, *J. Chem. Phys.* **79**, 6308 (1983).
- <sup>13</sup>A. H. Mones and B. Post, *J. Chem. Phys.* **20**, 755 (1952).
- <sup>14</sup>A. K. Wolf, J. Glinemann, L. Fink, E. Alig, M. Bolte, and M. U. Schmidt, *Acta Cryst. B* **66**, 229 (2010).
- <sup>15</sup>A. J. Valerga and J. E. Kilpatrick, *J. Chem. Phys.* **52**, 4545 (1970).
- <sup>16</sup>B. Krebs, G. Henkel, and M. Dartmann, *Acta Cryst. C* **45**, 1010 (1989).
- <sup>17</sup>H. Fleischer, S. Parsons, and C. R. Pulham, *Acta Cryst. E* **59**, m11 (2003).
- <sup>18</sup>W. Müller-Warmuth, K. H. Duprée, and M. Prager, *Z. Naturforsch. A: Phys. Sci.* **39**, 66 (1984).
- <sup>19</sup>M. Prager, K. H. Duprée, and W. Müller-Warmuth, *Z. Phys. B* **51**, 309 (1983).
- <sup>20</sup>D. M. Adams and M. Pogson, *J. Phys. C* **21**, 1065 (1988).
- <sup>21</sup>J. J. Rush and W. C. Hamilton, *Inorg. Chem.* **5**, 2238 (1966).
- <sup>22</sup>D. M. Adams and J. Haines, *Spectrochim. Acta, Part A* **49**, 237 (1993).
- <sup>23</sup>R. Gajda and A. Katrusiak, *Cryst. Growth Des.* **8**, 211 (2008).
- <sup>24</sup>N. W. Ashcroft, *Phys. Rev. Lett.* **92**, 187002 (2004).
- <sup>25</sup>J. Feng, W. Grochala, T. Jaron, R. Hoffmann, A. Bergara, and N. W. Ashcroft, *Phys. Rev. Lett.* **96**, 017006 (2006).
- <sup>26</sup>C. J. Pickard and R. J. Needs, *Phys. Rev. Lett.* **97**, 045504 (2006).
- <sup>27</sup>Y. Yao, J. S. Tse, Y. Ma, and K. Tanaka, *Europhys. Lett.* **78**, 37003 (2007).
- <sup>28</sup>O. Degtyareva, M. Martinez-Canales, A. Bergara, X. J. Chen, Y. Song, V. V. Struzhkin, H. K. Mao, and R. J. Hemley, *Phys. Rev. B* **76**, 064123 (2007).
- <sup>29</sup>X. J. Chen, J. L. Wang, V. V. Struzhkin, H. K. Mao, R. J. Hemley, and H. Q. Lin, *Phys. Rev. Lett.* **101**, 077002 (2008).
- <sup>30</sup>X. J. Chen, V. V. Struzhkin, Y. Song, A. F. Goncharov, M. Ahart, Z. X. Liu, H. K. Mao, and R. J. Hemley, *Proc. Natl. Acad. Sci. U.S.A.* **105**, 20 (2008).
- <sup>31</sup>M. I. Erements, I. A. Trojan, S. A. Medvedev, J. S. Tse, and Y. Yao, *Science* **319**, 1506 (2008).
- <sup>32</sup>D. Y. Kim, R. H. Scheicher, S. Lebègue, J. Prasongkit, B. Arnaud, M. Alouani, and R. Ahuja, *Proc. Natl. Acad. Sci. U.S.A.* **105**, 16454 (2008).
- <sup>33</sup>M. Martinez-Canales, A. R. Oganov, Y. Ma, Y. Yan, A. O. Lyakhov, and A. Bergara, *Phys. Rev. Lett.* **102**, 087005 (2009).
- <sup>34</sup>O. Degtyareva, J. E. Proctor, C. L. Guillaume, E. Gregoryanz, and M. Hanfland, *Solid State Commun.* **149**, 1583 (2009).
- <sup>35</sup>Y. Yan, J. Gong, and Z. G. Zong, *Chem. Phys. Lett.* **27**, 017401 (2010).
- <sup>36</sup>M. Martinez-Canales, A. Bergara, J. Feng, and W. Grochala, *J. Phys. Chem. Solids*, **67**, 2095 (2006).
- <sup>37</sup>Z. Li, W. Yu, and C. Jin, *Solid State Commun.* **143**, 353 (2007).
- <sup>38</sup>G. Gao, A. R. Oganov, A. Bergara, M. Martinez-Canales, T. Cui, T. Itaka, Y. Ma, and G. Zou, *Phys. Rev. Lett.* **101**, 107002 (2008).
- <sup>39</sup>C. Zhang, X. J. Chen, Y. L. Li, V. V. Struzhkin, R. J. Hemley, H. K. Mao, R. Q. Zhang, and H. Q. Lin, *J. Supercond. Novel Magn.* **23**, 717 (2010).
- <sup>40</sup>C. Zhang, X. J. Chen, Y. L. Li, V. V. Struzhkin, H. K. Mao, R. Q. Zhang, and H. Q. Lin, *Europhys. Lett.* **90**, 66006 (2010).
- <sup>41</sup>J. S. Tse, Y. Yao, and Y. Ma, *J. Phys.: Condens. Matter* **19**, 425208 (2007).
- <sup>42</sup>J. S. Tse, Y. Yao, and K. Tanaka, *Phys. Rev. Lett.* **98**, 117004 (2007).
- <sup>43</sup>P. Gonzalez-Morelos, R. Hoffmann, and N. W. Ashcroft, *Chem. Phys. Chem.* **11**, 3105 (2010).
- <sup>44</sup>G. Gao, A. R. Oganov, P. Li, Z. Li, H. Wang, T. Cui, Y. Ma, A. Bergara, A. O. Lyakhov, T. Itaka, and G. Zou, *Proc. Natl. Acad. Sci. U.S.A.* **107**, 1317 (2010).
- <sup>45</sup>P. Zaleski-Ejgierd, R. Hoffmann, and N. W. Ashcroft, *Phys. Rev. Lett.* **107**, 037002 (2011).
- <sup>46</sup>M. Hanfland, J. E. Proctor, C. L. Guillaume, O. Degtyareva, and E. Gregoryanz, *Phys. Rev. Lett.* **106**, 095503 (2011).
- <sup>47</sup>T. A. Strobel, A. F. Goncharov, C. T. Seagle, Z. X. Liu, M. Somayazulu, V. V. Struzhkin, and R. J. Hemley, *Phys. Rev. B* **83**, 144102 (2011).
- <sup>48</sup>Z. X. Qin, J. B. Zhang, I. Troyan, T. Palasyuk, M. Erements, and X. J. Chen, *J. Chem. Phys.* **136**, 024503 (2012).
- <sup>49</sup>Z. X. Qin, C. Zhang, L. Y. Tang, G. H. Zhong, H. Q. Lin, and X. J. Chen, *Phys. Rev. B* **86**, 184110 (2012).
- <sup>50</sup>M. P. Brown, R. Ogawara, and E. C. Rochow, *Spectrochim. Acta* **16**, 595 (1960).
- <sup>51</sup>Y. Lin, W. L. Mao, V. Drozd, J. H. Chen, and L. L. Daemen, *J. Chem. Phys.* **129**, 234509 (2008).
- <sup>52</sup>A. C. Larson and R. B. Von-Dreele, GSAS-General Structure Analysis System. Report LAUR 86-748. Los Alamos National Laboratory, USA. 1994.
- <sup>53</sup>G. Kresse and J. Furthmüller, *J. Comput. Mater. Sci.* **6**, 15 (1996).
- <sup>54</sup>G. Kresse and D. Joubert, *Phys. Rev. B* **59**, 1758 (1999).
- <sup>55</sup>D. M. Ceperley and B. J. Alder, *Phys. Rev. Lett.* **45**, 566 (1980).
- <sup>56</sup>R. B. Aust, W. H. Bentley, and H. G. Drickamer, *J. Chem. Phys.* **41**, 1856 (1964).
- <sup>57</sup>X. J. Chen, C. Zhang, Y. Meng, R. Q. Zhang, H. Q. Lin, V. V. Struzhkin, and H. K. Mao, *Phys. Rev. Lett.* **106**, 135502 (2011).
- <sup>58</sup>A. I. Kitajgorodski, *Kryształy Molekularne* (Warsaw, PWN, 1976) (in polish).
- <sup>59</sup>F. Birch, *Phys. Rev.* **71**, 809 (1947).
- <sup>60</sup>Y. Li, G. Gao, Y. Xie, Y. Ma, T. Cui, and G. Zou, *Proc. Natl. Acad. Sci. U.S.A.* **107**, 15708 (2010).
- <sup>61</sup>T. A. Strobel, M. Somayazulu, and R. J. Hemley, *Phys. Rev. Lett.* **103**, 065701 (2009).
- <sup>62</sup>M. S. Anderson and C. A. Swenson, *Phys. Rev. B* **10**, 5184 (1974).
- <sup>63</sup>S. Ishmaev, I. P. Sadikov, A. A. Chernyshov, B. A. Vindryaevskii, V. A. Sukhoparov, A. S. Telepnev, and G. V. Kobelev, *Zh. Eksp. Teor. Fiz.* **84**, 394 (1983). [*Sov. Phys. JETP* **57**, 228 (1983)].
- <sup>64</sup>H. K. Mao, A. P. Jephcoat, R. J. Hemley, L. W. Finger, C. S. Zha, R. M. Hazen, and D. E. Cox, *Science* **239**, 1131 (1988).
- <sup>65</sup>R. J. Hemley, H. K. Mao, W. Finger, A. P. Jephcoat, R. M. Hazen, and C. S. Zha, *Phys. Rev. B* **42**, 6458 (1990).
- <sup>66</sup>M. I. Erements and I. A. Trojan, *Nat. Mater.* **10**, 927 (2011).
- <sup>67</sup>R. T. Howie, C. L. Guillaume, T. Scheler, A. F. Goncharov, and E. Gregoryanz, *Phys. Rev. Lett.* **108**, 125501 (2012).
- <sup>68</sup>C. S. Zha, Z. X. Liu, and R. J. Hemley, *Phys. Rev. Lett.* **108**, 146402 (2012).